



## The impacts of dust aerosol and convective available potential energy on precipitation vertical structure in eastern China as seen from multiple source observations

Hongxia Zhu<sup>1</sup>, Rui Li<sup>1,2,3</sup>, Shuping Yang<sup>1</sup>, Chun Zhao<sup>1</sup>, Zhe Jiang<sup>1</sup>, and Chen Huang<sup>1</sup>

5 <sup>1</sup>School of Earth and Space Science, Comparative Planetary Excellence Innovation Center, University of Science and Technology of China, Hefei 230026, China

<sup>2</sup>State Key Laboratory of Fire Science, University of Science and Technology of China, Hefei 230026, China

10 <sup>3</sup>Institut de recherche sur les forêts, Université du Québec en Abitibi-Témiscamingue (UQAT), Rouyn-Noranda, J9X 5E4, Canada

Correspondence to: Rui, Li ([rli7@ustc.edu.cn](mailto:rli7@ustc.edu.cn))

**Abstract.** The potential impacts of dust aerosol and atmospheric convective available potential energy (CAPE) on the vertical development of precipitating clouds in eastern China were studied using multiple-sources observations. In the study area, heavy dusty condition is coupled with strong north wind which  
15 carried air mass contained high concentration of mineral dust particles with cold temperature and strong wind shear. This leads to weaker CAPE in dusty days comparing with that in pristine days. Based on satellite observations, the precipitating drops under dusty condition grow faster at middle layer (with temperature -5 °C to +2 °C) but slower at upper and lower layer comparing with the pristine counterpart. For a given precipitation top height, the precipitation rate under dusty condition is weaker in upper layer  
20 but heavier at middle and lower layer. And the associated latent heating rate released by precipitation at middle layer is stronger. The precipitation top temperature (PTT) shows fairly good linear relationship with near surface rain rate (NSRR). The linear regression slope between PTT and NSRR are stable at dusty and pristine conditions. However, the  $PTT_0$  (precipitation top temperature related to rain onset) at the onset of rain are highly affected by both CAPE and aerosol condition. In pristine days, stronger CAPE  
25 facilitate the vertical development of precipitation and leads to a decrease of  $PTT_0$  at the rate of -0.65 °C per 100 J kg<sup>-1</sup> CAPE for deep convective precipitation with variation of 15 %, and by -0.41 °C per 100 J kg<sup>-1</sup> CAPE for stratiform precipitation with variation of 12 %. After removing the impacts of CAPE on PTT, dust aerosols lead an increase of PTT at the rate by +4.19 °C per unit AOD for deep convective precipitation and by +0.35 °C per unit AOD for stratiform precipitation. This study showed clear



30 evidence that meteorology conditions are combined with aerosol condition together to affect the vertical development of precipitation clouds. And quantitative estimation of the sensitivity of PTT to CAPE and dust were provided.

## 1 Introduction

Dust aerosols are widely distributed in the troposphere, they can scatter and absorb solar shortwave radiation and terrestrial longwave radiation to directly affect the global radiation budget (Bellouin et al., 2005; Huang et al., 2014). On the other hand, dust aerosols can act as ice nuclei (IN, Demott et al., 2003; Atkinson et al., 2013; Li et al., 2017a) to enhance heterogeneous freezing process and favorite ice formation at relatively warmer temperature and lower vapor saturation ratio. In addition, dust particles coated with water soluble pollutants can server as cloud condensation nuclei (CCN, Yin and Chen, 2007; Li et al., 2010) to decrease effective radius of cloud droplets for given liquid water content and indirectly moderate warm rain process. The mechanisms of dust aerosol affecting atmospheric hydrometers are distinct at different temperatures and altitudes.

Observational studies of dust aerosols affecting clouds and precipitation at different vertical layers has received increasing attentions in recent years. In particular, the observations of the vertical structure of precipitation by spaceborne precipitation radar make it possible to investigate in detail the impacts of dynamics and aerosols on cloud and rain formation at different heights and temperatures. Studies have shown that the vertical structure of precipitation is influenced by aerosols in addition to dynamic conditions (Min et al., 2009; Li and Min, 2010; Fan et al., 2013, 2018; Rosenfeld et al., 2014; Gibbons et al., 2018; Chen et al., 2016; Guo et al., 2018; Wall et al., 2015). In a case study of the interaction between Sahara dust and mesoscale convective system over equatorial Atlantic Ocean, Min et al. (2009) found that convective precipitation rate in dust laden sector was weaker than that in pristine environment; and the radar echoes of stratiform precipitation influenced by dust were stronger at upper levels than those in a pristine environment. Li and Min (2010) further analyzed the variation of precipitation rate with height and found the impacts of mineral dust on tropical cloud and precipitation systems are highly dependent on rain type. The convective rain rate weakened at all heights, but stratiform precipitation showed enhanced rain rate above 6 km, in dust laden area, indicating that dust aerosols enhanced the heterogeneous ice nucleation process. In their study, variations of precipitation related to meteorology



conditions were constrained by fixing the rain types, the precipitation top height etc. Gibbons et al. (2018) used cloud resolving model simulations to reveal that more and smaller ice particles release more latent  
60 heat (LH) during deposition growth and riming after being affected by dust, promoting convective development. During diffusional growth, competition for available water vapor from more particles reduces the particle growth rate, shifting the height of precipitation formation to higher heights during heterogeneous nucleation regime. In addition, Guo et al. (2018) found that convective precipitation in polluted conditions had deeper and stronger radar reflectivity pattern, while stratiform and shallow  
65 precipitation had shallower and weaker pattern than those under clean conditions.

The precipitation top height/temperature (PTH/PTT) is one of the most important parameters to represent the vertical structure of precipitation. It is mainly controlled by the strength of the updraft (Nasuno and Satoh, 2011). In addition, the colder PTT (the higher PTH), the longer falling path of precipitation drops and the stronger rain rate can be reached at the surface (Cao and Qi, 2014; Liu and Fu, 2001). Li et al.  
70 (2011b) found that for mixed-phase clouds, the cloud top height increases with the concentration of condensation nuclei, for water clouds, the cloud top height is insensitive to condensation nuclei. Dong et al. (2018) studied the effect of Sahara dust aerosols on PTH in the equatorial Atlantic Ocean, and found for a given near surface rain rate (NSRR), the PTH of stratiform precipitation in dusty condition was significantly higher than its pristine counterpart. In that study, it was found the variations of rain fall  
75 vertical structure was dominated by dynamics which can explain about 90 % variance. Guo et al. (2018) found that the mean top heights of 30 dBZ radar reflectivity of polluted convective (stratiform) precipitation increased (decreased) by ~29% (~10.8%) compared to that under clean conditions.

The spatial distribution of aerosols significantly was affected by meteorological conditions (Oshima et al., 2012). Such as convective transport (Prospero and Mayol-Bracero, 2013), wet removal processes  
80 (Park and Allen, 2015), boundary layer height and evolution processes (Li et al., 2017b). Aerosol-cloud-precipitation interactions (ACIs) also largely depend on meteorology conditions including wind shear (Fan et al., 2009, 2013), atmospheric stability (Huang et al., 2014), relative humidity (Li et al., 2019b), and the altitudes of the aerosol layer (Yin et al., 2012).

Fan et al. (2013) found that the thermodynamic effect of aerosols (freezing of cloud water to release  
85 additional latent heating) contributes up to 27 % to the increase in cloud cover during the growth stage of deep convective clouds in summer, while the microphysical effect of aerosols (freezing of large



amounts of cloud droplets to produce more and smaller ice particles) increases cloud cover and cloud top height during the mature and dissipation stages. In addition, weather conditions and dust aerosols have important effects on the vertical structure of precipitation. Khain (2009) found that strong wind shear  
90 within clouds detaches ice particles and small droplets from the updraft zone and transports them downwind from the cloud updraft, allowing particles to fall and evaporate in relatively dry air. The wind shear at lower levels can slow down the flow inside the atmospheric convective boundary and enhances the entrainment process (Fedorovich and Conzemius, 2008), which leads to stronger evaporation, faster sublimation rates and greater evaporative cooling, which in turn suppresses convective intensity. When  
95 the atmosphere is wetter, the reduction of net latent heat released by aerosols is larger and the rate of reduction of convective intensity with increasing aerosols is greater in wet air than in dry air (Fan et al., 2009). Zhang et al. (2012) found that dust can increase the ice concentration in midlevel supercooled stratiform clouds by a factor of 2 to 6 at temperatures colder than  $-12\text{ }^{\circ}\text{C}$ . And this enhancement was strongly dependent on cloud top temperature, concentration of dust particles and chemical composition.

100 A great challenge in observational study on the indirect effects of aerosols is the difficulty of distinguishing between the differential contributions of weather conditions (dynamic conditions) and aerosol microphysical effects to the observed macro-micro features of clouds and precipitation. This is especially true for mesoscale convective systems (MCSs) that are heavily affected by large-scale atmospheric circulation. In some studies, it were actually assumed that the dynamic conditions are the  
105 same in cloud and precipitation samples under different aerosol conditions, or that the dynamic conditions do not have a significant difference impacts on the observed features. There is no theoretical or practical evidence to support such hypothesis. On the contrary, for areas far from the source of a certain type of aerosol (such as mineral dust), the occurrence of high aerosol concentrations is often accompanied by specific atmospheric circulation conditions (for long-distance transport of aerosols), then at this  
110 circumstance, the observed cloud and precipitation characteristics are jointly determined by the combination of obviously different aerosol conditions and weather conditions, if we want to understand the pure indirect effects of aerosols, we will have to untangle these two different effects.

To this end, this study specially selected southeast China as the research area. It is relatively far from the original source of dust, so a relatively fixed atmospheric circulation condition (northwest wind) is  
115 required to transport dust to this area, which creates an ideal test bed for us to investigate combined



effects from dust aerosol and meteorology conditions on precipitation. Particularly, this study investigates the effects of convective available potential energy (CAPE) and dust aerosol on the processes of precipitation particle formation, LH releasing, and the macrophysical vertical features of precipitation in the Southeastern China. In addition, the sensitivity of PTT to CAPE and aerosol optical depth were  
120 quantitatively studied.

## 2 Study Area and Data

The Southeastern China (110° E-125° E; 20° N-30° N) was selected as the study area. It is featured by strong and frequent summer precipitation and is far from the terrestrial dust original source. Therefore, the potential dust-precipitation interaction must occur under special weather condition. This is useful for  
125 us to investigate the separated effects from aerosol and thermodynamics on clouds. And the study focused on precipitations in June, July and August (JJA) during 2000 to 2013.

The standard product 2A25 of Tropical Rainfall Measuring Mission (TRMM) was utilized in this study (Iguchi et al., 2000) with 4.3-km horizontal and 250-m vertical resolutions at nadir. From up to down, the height of the first three continuous vertical bins with PR detectable echoes are defined as precipitation  
130 top. And the associated air temperature (see below data collocation method) are defined as PTT. As mentioned by Houze (1997), the dynamic condition associated with convective and stratiform precipitation are so different, they are treated separately in this study. Each precipitation profile has a certain rain type of convective, stratiform or others (Awaka et al., 1997). Because the dynamic conditions in convective and stratiform precipitation are different (Houze, 1997), and the potential dust related  
135 effects are also distinct (Li et al., 2017a; Li and Min, 2010), those two types of precipitation are investigated separately in this study. In addition, warm rains were separated from the two types. Warm rain is defined as those with precipitation top temperature warmer than 0 °C. Teller and Levin (2006) found that dust can act as giant CCN to enhance collision and coalescence during droplet growth, thus enhancing warm precipitation. Yin and Chen (2007) found that dust-induced heating inhibits cloud  
140 droplet formation and precipitation development when dust occurs at altitudes warmer than -5 °C.

Based on satellite radar observations (Liu and Fu, 2001), from the rain top to the surface, the precipitation rate ( $R$ , unit  $\text{mm h}^{-1}$ ) at logarithm (i.e.  $\log R$ ) changes linearly with the decreasing height ( $H$ ) piece wisely in three vertical layers. At the highest level, precipitation particle growth relies primarily on the water



vapor deposition process, the growth rate is slow, and the linear regression slope of the logR to H is small.

145 In the layer of about 1.5-2 km above and below the freezing level, precipitation particles rely on the process of aggregation, and riming to grow rapidly, and the corresponding linear regression slope is large. In the lower layer, the convective precipitation rate shows a further slight increase due to coalescence with cloud droplets with very small linear regression slope. The stratiform precipitation rate in this layer is basically no longer growing due to the lack of cloud droplets. Both of convective and stratiform

150 precipitation rate may decrease towards ground due to particle break-up and evaporation. Li et al. (2011a) found above phenomenon standing valid when changing the vertical coordinate from height (H) to temperature (T). They further defined the associated logR~T linear regression slopes ( $\partial \log R / \partial T^{-1}$ ) as 1) SlopeA in the layer with temperatures colder than -5 °C, 2) SlopeB in the middle layer with temperatures between -5 °C to 2 °C, and 3) SlopeC in the lowest layer with temperatures warmer than 2 °C, respectively.

155 It was found the three slopes respond to variations of atmospheric dynamics and thermodynamics related to El Nino. In this study, we adopted the definition of Slopes A, B, C to study the growth rate at upper, middle and lower layers.

The formation of precipitation is accompanied by the release or depletion of latent heat (LH), which plays an important role in maintaining the global energy balance (Houze, 1997; Li et al., 2019a). The

160 standard TRMM 2A25-base LH products derived from Convective and Stratiform Heating algorithm (CSH, Tao et al., 1993, 2010), Spectrum Latent Heating algorithm (SLH, Shige et al., 2004, 2007), and the recently developed Vertical Profile Heating algorithm (VPH, Li et al., 2011a, 2019a) were used in this study to investigate the possible impacts of aerosols on precipitation LH.

The standard aerosol product MOD04\_3K AOD from Terra MODIS at horizontal resolution of 3 km

165 were used in this study. The retrieved aerosol optical thickness (AOD), the fine mode fraction (FMF) and the coarse mode AOD (CMAOD= AOD×(1-FMF)) were combined to define dusty and pristine conditions. Because AOD is not available under cloudy sky, for each 1×1 grid where precipitation were detected by TRMM PR, the averaged AOD and CMAOD from the surrounding eight grids are assigned to this grid. Then the mean CMAOD from all precipitating grids at the same day were calculated. If the

170 mean CMAOD is larger than 0.5, then the day was defined as “dusty day”. If the mean total AOD is less than 0.2, the day was defined as pristine day.



The atmospheric thermodynamic conditions under pristine or dusty environments were derived from hourly ERA5 reanalysis data at horizontal resolution of  $0.25^\circ \times 0.25^\circ$ . The parameters including air temperature (T), zonal wind field (U) and meridional wind field (V) at the upper (300 hPa), middle (500 hPa) and lower (750 hPa) level and Convective Available Potential Energy (CAPE) are investigated.

### 3 Results

#### 3.1 The coupling between aerosol conditions and meteorology conditions

The selected study area is undergoing fast economic development during recent two decades. In summer, the area generally was dominated by anthropogenic emission related fine mode aerosols with small fraction of coarse mode aerosol (Fig. 1a, b, c--- total AOD, CMAOD and FMAOD in all days). However, still there are some days heavy dust aerosol in this area can be observed by satellite with high value of coarse mode AOD (Fig. 1d-f). During 2000-2013 JJA, there are 46 raining days were defined as dusty condition with CMAOD exceeded 0.5 averaged from raining pixels. Meanwhile, 92 raining days were defined as pristine condition with area mean total AOD smaller than 0.2.

The study area is not the original emission source of mineral dust, instead, the satellite observed dust was transported from remote desert areas. Special large scale atmospheric circulation conditions are required to show significant dust aerosol in this area. For example, on 12 June 2006 a typical dusty day, about half of the study area was covered by heavy dust (Fig. 2) with satellite observed CMAOD up to 1. The back trajectory analysis using HYSPLIT (Fig. 2) showed the dusty air mass were coming from the Gobi and/or Taklamakan Desert.

Large scale circulations at 300, 500, and 750 hPa for dusty and pristine days were analyzed (Figs. 3 and S1). Generally, the dust emission source area in northern China is under the control of the westerly wind. When the selected study area was in dusty conditions, in  $35^\circ\text{N}$  -  $50^\circ\text{N}$  belt the southward wind component was significantly strengthened, which transported the dust aerosol southwardly into the study area (Fig. S1). At the same time, it also transported colder air masses from the north to the south, resulting in temperature at 500 hPa about 1 degree colder than that in the pristine condition. In addition, when the study area was in the dusty condition, the 1000-500 hPa layer U wind shear was about 2 times of that in pristine condition ( $5.1 \text{ m s}^{-1}$  vs.  $2.9 \text{ m s}^{-1}$ ). Finally, as an overall measure of regional mean atmospheric dynamic conditions, regional CAPE was  $600 \text{ J kg}^{-1}$  in dust conditions and  $743 \text{ J kg}^{-1}$  in clean conditions.



200 In summary, strong coupling between dusty condition and meteorology condition are observed based on  
above analysis. The spatial correlation coefficient between CMAOD and CAPE is -0.07, and is -0.08 for  
CMAOD against T (700 hPa), 0.09 for CMAOD against U windshear, and 0.07 for U wind at 700 hPa,  
respectively. Comparing the dusty condition to the pristine condition, its CAPE is lower, the air  
temperature is colder, the U wind shear is stronger, and the north wind is enhanced. Such condition  
205 doesn't favor the vertical development of convection. In the following discussion, the CAPE were used  
as an overall indicator for investigating the impacts of meteorology condition on precipitation features.

### 3.2 Differences in vertical profiles of precipitation

The precipitation vertical profiles, i.e., the function of the precipitation rate changing with the vertical  
height (temperature), contains information of precipitating particles growing mechanisms and speed  
210 during the falling from precipitation top to the surface ( Liu and Fu, 2001). Li et al. (2011a) further  
discussed how this profile can be affected by large-scale circulations, such as those in the different phases  
of ENSO. Li et al. (2019a) directly uses the vertical gradient of precipitation rate to estimate the latent  
heating rate in clouds. However, few study reported the possible effects of dust aerosols on the shape of  
precipitation profiles.

215 It is expected that changes in dynamic conditions will lead to changes in the precipitation profile. As  
shown in Fig. 4a-b, for a given NSRR, the precipitation top temperature (height) in pristine conditions  
(dotted curves) are colder (higher) than those in dusty conditions (solid curves) for deep stratiform and  
convective precipitation. In the layer from precipitation top to about -10 to -5 °C , the mean precipitation  
rates in pristine condition are heavier than those under dusty condition. However, in next layer when  
220 temperature is ranging from -5 °C to 2 °C, the precipitation rate in dusty condition grows much faster  
than that in pristine condition. The effect is so significant that the dusty precipitation rate exceeds pristine  
precipitation rate at about 0 °C and keep growing rapidly. In the lowest layer close to surface,  
precipitation rate under dusty condition grows slower.

From another viewing angle, when dropping from the same PTTs (Fig. 4d, e), the precipitating particles  
225 in dusty condition grow slower than its pristine counterpart at upmost layer. Start from temperature  
around -10 °C to -5 °C , the dusty precipitating particles grow faster and obtained large amount of water  
mass in the middle layer. Although followed by a layer with slower growing, the final NSRR for given  
PTT under dusty condition (solid curve) still is much heavier than that of pristine rains (dotted curve).





For the warm rains without ice phase microphysical processes, for given NSRR, colder PTT is required  
230 for dusty rains (Fig. 4c). When dropping from the same PTT, dusty rain rate increases slower than pristine  
rain and is weaker at the near surface (Fig. 4f). This indicates a possible suppression by dusty condition  
for warm rain growth.

Accompanied with the changes of vertical profiles, the latent heating released from dusty precipitation  
also are changed comparing to the pristine precipitation. Figure 5 represents the contoured frequency by  
235 altitude diagrams (CFAD) of LH (retrieval from VPH method) for deep stratiform rains and convective  
rains, respectively. Under dusty conditions, stratiform and convective rains exhibits an increased positive  
heating near 5 km altitude and a decrease of heating at higher layer. Meanwhile, the cooling (i.e. negative  
LH) in layer lower than 5 km is also enhanced based on Fig. 5c and 5f.

Figure 6 shows the mean LH profiles for stratiform and convective precipitation derived from the three  
240 different LH algorithms (i.e. SLH, CSH and VPH). For stratiform rains, there is no significant difference  
between SLH and CSH between pristine and dusty precipitations at all heights, while VPH shows a  
stronger latent heat in the dusty condition near 5-6 km.

For deep convective rains, VPH shows that the LH in the dusty condition is weaker than that in the  
pristine environment in the upper layers above 8 km, while is stronger in the middle layers around 5-6  
245 km. Both CSH and SLH showed neglectable differences at upper layer, but also showed stronger LH in  
dusty condition in middle layer and lower layers comparing to pristine condition.

There are significant differences of mean LH profiles among the three algorithms indicating still large  
uncertainties in satellite retrieval of LH. However, all the three products agree that LH in deep convective  
precipitation at middle layer (around 5-6 km) in dusty condition should be stronger than those in pristine  
250 condition.

### 3.3 Differences in the growth rate of precipitation

In this section we adopted the same method of Li et al. (2011a) to use the linear regression slope of  
precipitation rate (at logarithm) to temperature (i.e.  $d\log R dT^{-1}$ ) to quantify the differences of growth rate  
at different layers between dusty and pristine conditions. We only focus on deep convective and stratiform  
255 rains in this section.

In a NSRR-PTT space, the mean SlopeA (upper layers), SlopeB (middle layers), and SlopeC (lower  
layers) under pristine and dusty conditions were compared as shown in Figs. 7 and 8.



For a given NSRR, all slopes decrease with decreasing PTT (i.e. increasing precipitation top height). For a given PTT, SlopeA and SlopeB increase with NSRR, while SlopeC is almost insensitive to NSRR. This indicates the growth rate at upper layer and middle layer are critical to determine the final surface rain rate. It should be noticed that even both PTT and NSRR are constrained, still SlopeB in dusty conditions is significantly stronger than that in pristine conditions (Figs. 7f and 8f), meanwhile, SlopeA is not significantly different, and SlopeC is weaker in dusty conditions than that in pristine conditions.

For a given PTT, mean SlopeA of pristine stratiform precipitation (dash curve) is slightly greater than for dusty precipitation (Fig. 9a). However, Slope B for both convective and stratiform rains in dusty condition are remarkably greater than its pristine counterpart (Fig. 9c, d). And the t testing showed that most differences of SlopeB exceeded the 95 % or 99 % confidence level (Fig. S2). This finding strongly supports the hypothesis that dust aerosol enhanced the heterogeneous freezing process at temperature much warmer than  $-38\text{ }^{\circ}\text{C}$  (the threshold for homogeneous freezing). There are more ice phase hydrometeors in the middle layer of dusty condition to favor the aggregation and rimming process so that precipitation drops can grow faster than those in pristine condition. And the slightly smaller Slope A for dusty condition can be explained that the fast formation of cloud and precipitation in middle layer exhaust water vapor at middle layer, few water vapor at upper layer can be used for precipitation growth in dust condition.

In the lowest layer, when precipitation particles fall to the ground, the SlopeC of stratiform precipitation is basically negative (Fig. 9e), which corresponds to the evaporative and/or breakup process of raindrops. From the analysis in Section 3.1, it is known that the dusty condition corresponds to a stronger U windshear (Fig. 3d-f), and the stronger windshear may enhance the evaporative and/or breakup processes (Fan et al., 2009, 2013; Li et al., 2010). It was confirmed in Fig. 9 that the SlopeC of stratiform rains in dusty condition is more negative than that in pristine condition. For convective precipitations in the lowest layer, raindrops still can slightly increase through the coalescence of cloud droplets. Based on the observations, the SlopeC of convective rains in dusty condition is smaller than pristine condition, indicating the coalescence process of cloud droplets was suppressed. The strong windshear in the dusty condition may cause this suppression. In addition, polluted dust particles may also act as CCN to decrease the effective radius of cloud droplets and inhibit the coalescence efficiency as suggested by Rosenfeld (2008) and Li et al. (2010).



### 3.4 The sensitivity of PTT to CAPE and aerosol

Precipitation top temperature (PTT) has a close relationship with surface rain rate (NSRR) because the higher PTT is related to longer falling pathway and more cloud droplets can be collected, consequently, thus heavier NSRR can be reached. However, the formation of ice and liquid cloud droplets, the growing mechanisms, and the collision efficiencies all can be modified by both dynamical, thermodynamical, and microphysical processes. Aerosols, either acting as CCN or IN also have potential capability to moderate the quantitative relationship between PTT and NSRR.

The PTT-NSRR relationships for stratiform, convective and warm rains in pristine (dotted line) and dusty (solid line) conditions, and for different level of CAPE are shown in Fig. 10. For given NSRR, the PTT in pristine conditions is colder than those in the dusty conditions (i.e., the precipitation top is higher). For given PTT, the precipitation rate NSRR under dusty conditions is stronger than that under pristine conditions. This confirmed that the changes in the microphysical processes (e.g., Figs. 7 and 8) induced by dust aerosol can lead to measurable changes in precipitation characteristics at the macroscopic scale. CAPE is one of the most representative parameters of atmospheric dynamical conditions and can reflect the overall stability of the atmosphere, which was widely used to quantify the dynamical constraint on convection development in aerosol cloud interaction studies (e.g. Doswell and Rasmussen, 1994). We tested the impacts of CAPE on PTT-NSRR relationship in pristine samples to alleviate the tangling effects from aerosol.

All pristine stratiform and convective raining samples are divided into two groups with strong CAPE (i.e. over  $700 \text{ J kg}^{-1}$  for stratiform rains and over  $1100 \text{ J kg}^{-1}$  for convective rains) and weak CAPE (i.e. weaker than  $350 \text{ J kg}^{-1}$  for stratiform rains and  $700 \text{ J kg}^{-1}$  for convective rains) to check the impacts of dynamic conditions on the PTT-NSRR relationship. As shown in Fig. 10d-f, CAPE change the relationship between NSRR and PTT. For a given NSRR, PTTs under stronger CAPE (gray curves) is about 5-6 (2.0) degree colder than those under weaker CAPE (black curves) in both stratiform and convective rains (warm rains) under pristine conditions. The t-testing significances of difference exceeded the 99 % confidence level (Fig. S3). It indicates that strong dynamical conditions will favor raindrops reaching high altitudes with colder PTTs. Meanwhile, it was found the linear regression slope are similar between different CAPEs. It indicates the growth rates of rain drops along the falling path are similar under pristine environment, therefore the increase of NSRR is proportional to the increase of PTT.



Since the satellite observations showed PTT has a good linear relationship with NSRR (Fig. 10), the PTT can be expressed as a linear function of NSRR:

$$PTT = PTT_0 + K \times NSRR, \quad (1)$$

where  $PTT$  is the precipitation top temperature ( $^{\circ}\text{C}$ ),  $NSRR$  is the near surface rain rate ( $\text{mm h}^{-1}$ ),  $K$  is the linear regression slope, and  $PTT_0$  is the intercept when NSRR equals to zero. Physically,  $PTT_0$  represents the precipitation top temperature related to rain onset (when NSRR equals to zero), and  $K$  represents the sensitivity of PTT to NSRR. Previous investigations demonstrate that  $K$  is relatively stable for different CAPES or aerosol conditions, so that we mainly focus on the variations of  $PTT_0$ .

Cloud dynamics and aerosol-related microphysics combinedly affect the PTT-NSRR relationship. For the difference of  $PTT_0$  between two groups of samples with different CAPE and dust AOD, We separate the difference of  $PTT_0$  as a follows

$$\Delta PTT_0 = \frac{\partial PTT_0}{\partial CAPE} \Delta CAPE + \frac{\partial PTT_0}{\partial AOD} \Delta AOD, \quad (2)$$

where  $\frac{\partial PTT_0}{\partial CAPE}$  represents the sensitivity of  $PTT_0$  to CAPE,  $\frac{\partial PTT_0}{\partial AOD}$  represents the sensitivity of  $PTT_0$  to aerosol.

Therefore, the term of

$$\frac{\partial PTT_0}{\partial AOD} = \frac{\Delta PTT_0 \frac{\partial PTT_0}{\partial CAPE} \Delta CAPE}{\Delta AOD}. \quad (3)$$

To determine the sensitivity of  $\frac{\partial PTT_0}{\partial CAPE}$ , we randomly selected 70 % of the pristine precipitation samples (to avoid potential contaminations from aerosol effect) to investigate the relationship between  $PTT_0$  and CAPE. All the samples were sorted into 6 bins with increasing values of CAPE, and the sample size for each bin are general the same. In each bin, linear regression were conducted to determine  $K$  and  $PTT_0$  following the Eq. (1). To determine the uncertainty of this estimation, we repeated the randomly selecting processes 40 times. And all the results are shown in Fig. 11.

As we can see, the  $PTT_0$  showed a very strong linear correlation with CAPE. The determining factor are 0.78, 0.86 and 0.31 for deep stratiform, convective and warm precipitation, respectively. With increasing CAPE, cloud drops are easy to be elevated to higher altitude (low  $PTT_0$ ) and precipitation embryos start to form there.

Quantitatively, it was estimated that  $PTT_0$  decreases by  $0.41^{\circ}\text{C}$  per  $100 \text{ J kg}^{-1}$  CAPE (the linear regression slope in Fig. 11) for deep stratiform precipitation with variation of 12 % (standard deviation of the 40



times estimations of  $\frac{\partial PTT_0}{\partial CAPE}$  divided by the mean  $\frac{\partial PTT_0}{\partial CAPE}$ ). And  $PTT_0$  decreases by 0.65 °C per 100 J kg<sup>-1</sup>  
345 CAPE for deep convective precipitation with variation of 15 %. For warm rains,  $PTT_0$  decreases only by  
0.066 °C per 100 J kg<sup>-1</sup> CAPE but with large variation of 38 % indicating this method didn't work good  
for it.

Finally, substituting the estimated  $\frac{\partial PTT_0}{\partial CAPE}$ , the mean values of  $\Delta PTT_0$ ,  $\Delta AOD$ , and  $\Delta CAPE$  between  
dusty and pristine samples into the Eq. (3), the sensitivity of  $PTT_0$  to aerosol optical depth  $\frac{\partial PTT_0}{\partial AOD}$  was  
350 obtained. The  $PTT_0$  increases by 4.19 °C per unit AOD for deep convective precipitation and by 0.35 °C  
per unit AOD for stratiform precipitation. Results for warm rains were not shown here due to its large  
uncertainties.

#### 4 Discussion and conclusion

Mineral dust is a type of aerosol with the largest proportion of mass on land, and can act as both IN and  
355 CCN to affect clouds and precipitation. At present, the study of the indirect effects of dust aerosols on  
climate has shifted from qualitative to quantitative. It is expected that the effects of dust aerosols on  
clouds and precipitation can be accurately described in numerical models. A typical example is that  
Demott et al. (2010) directly wrote the number density of aerosols with an effective radius greater than  
0.5 microns (mainly dust) into the IN parameterized formulas in cloud resolution mode. However, the  
360 effectiveness of such model parameterization is hard to be assessed with large-scale satellite observations.  
The physical characteristics of cloud or precipitation in real observations are affected by both aerosol  
indirect effects (if any) and atmospheric thermodynamical effects. Unfortunately, to isolate those two  
types of effects is the most difficult part of observational study on the cloud aerosol interaction.

In this study, we selected southeast China, which is far from the original source of dust for study area.  
365 Here, heavy dust conditions are often accompanied by strong northwesterly winds, strong wind shear,  
cold air temperature, and weak CAPE. Such relatively fixed weather conditions facilitate the isolation of  
aerosol indirect effects from dynamic effects. In order to study the IN effect of dust, we selected the  
vertical profile of precipitation observed by the spaceborne rain radar measurements as the basic data.  
By coupling multi-source satellite data and reanalysis data, dusty precipitation samples and pristine



370 precipitation samples in June, July and August (JJA) during 2000 to 2013 were separated for comparative analysis.

First, it was found that there was a difference in the averaged vertical profile between dusty and pristine samples. For the same precipitation top temperature (PTT), the dusty precipitation rate was weaker than that of pristine precipitation in the upper layer; and in the middle layer, it was significantly larger than  
375 the pristine precipitation, and the precipitation rate near surface was also larger under the conditions of dust. By quantifying the rate of precipitation growth, it is found that in the upper layers, the growth of dusty precipitation is slower. But in the middle layer, the growth rate of dusty precipitation is remarkably faster than that of pristine precipitation. Qualitatively, these phenomena confirmed that mineral dust can enhance the heterogeneous freezing process and lead to observable changes in precipitation rate.

380 In this study area, heavy dusty condition is always coupled with strong wind shear, which favors evaporation process in the lower layers (temperatures warmer than 2 °C) of stratiform precipitation, corresponding to a stronger cooling. Stronger wind shear is also unfavorable to the warm rain process due to suppression of cloud droplet coalescence. Dust aerosols may delay the onset of weak precipitation in the lower layers, thus more water droplets are lifted to the middle layers (temperature -5 °C to 2 °C)  
385 where dust aerosols can act as additional ice nuclei to enhance heterogeneous freezing. Consequently, at middle layers, precipitation particles grow rapidly through aggregation and riming, releasing large amounts of additional latent heat.

As a macroscopic manifestation of the above microphysical processes, we found that for a certain surface precipitation rate, the PTT of dusty precipitation is warmer than that of pristine precipitation. This is a  
390 combination of specific weather conditions and potential aerosol indirect effects on dust days. Through data analysis, we found that for every 100 J kg<sup>-1</sup> decrease in CAPE, the onset PTT of convective precipitation and stratiform precipitation will increase by 0.65 and 0.41 degrees Celsius, respectively. This is the first reason for the warmer precipitation top temperature on dusty days. In addition, for every unit increase in the aerosol optical depth of dust aerosols in the atmosphere, the PTT of convective  
395 precipitation and stratiform precipitation will increase by 4.19 and 0.35 degrees Celsius, respectively. This is the second reason for the warmer temperature of the rain top of precipitation on dust days.

Based on our knowledge, this is the first time to separate the contribution of aerosol to satellite observed precipitation top temperature from real satellite observations. The results can be used to evaluate cloud



resolving model simulations and to assess the performance of model parametrizations related to dust  
400 aerosol IN effect.

It should be noticed there are several uncertainties in this study. First, the coarse mode aerosol AOD  
(CMAOD= AOD×(1-FMF)) is calculated from the MODIS observed AOD and the fine mode fraction  
(FMF or f). Jones and Christopher (2007) pointed out that the FMF spatial and temporal variations were  
not well considered and the resulting coarse particle AOD was too empirical, and the resulting coarse  
405 particle AOD may not accurately reflect the real atmospheric aerosol optical depth. Second, coarse mode  
aerosols are not necessarily dust aerosols either. There is still a lack of long-term, large-scale dust  
observation to solve this problem precisely. In addition, because AOD is not available under cloudy sky,  
for each 1×1 grid where precipitation was detected by TRMM PR, the averaged AOD from the  
surrounding eight grids are assigned to this grid. All above factors introduced uncertainties into the  
410 estimation of background dust-related AOD in raining pixels. In addition, the relationship between NSRR  
and PTT is influenced by multiple dynamic factors, such as upward velocity, water vapor, wind shear etc.  
In this study, we only analyzed the sensitivity of PTT to CAPE.

**Data availability.** Precipitation data are obtained from the Tropical Rainfall Measuring Mission (TRMM)  
415 satellite (<https://gpm.nasa.gov/missions/trmm>). The standard TRMM 2A25-base latent heat products  
derived from Convective and Stratiform Heating algorithm (CSH) and Spectrum Latent Heating  
algorithm (SLH) are available at <https://search.earthdata.nasa.gov/search?q=TRMM>. The latent heat  
products derived from vertical profile heating algorithms (VPH) are available from Hongxia Zhu  
(zhx227@mail.ustc.edu.cn). Aerosol optical thickness data are obtained from Moderate Resolution  
420 Imaging Spectroradiometer (MODIS) on Terra satellite (<https://modis.gsfc.nasa.gov/>). The data for the  
back trajectory analysis are obtained from Hybrid Single-Particle Lagrangian Integrated Trajectory  
(HYSPLIT) model (<https://www.ready.noaa.gov/hypub-bin/trajtype.pl?runtype=archive>). Hourly  
meteorological data are obtained from European Centre for Medium-Range Weather Forecasts ERA5  
reanalysis (<https://www.ecmwf.int/>).

425

**Author Contribution.** R. Li designed the experiments and H.X. Zhu and S.P. Yang carried them out. S.P.  
Yang and C. Huang conducted the latent heating retrieving. H.X. Zhu and R. Li prepared the manuscript  
with contributions from all co-authors.

430 **Competing interests.** The authors declare that they have no conflict of interest.

**Acknowledgements.** This work was supported by the National Natural Science Foundation of China  
(Grant No. 41830104, 41661144007, 41675022), National Key Research and Development Program of  
China (Grant No. 2021YFC3000301-1), and the Jiangsu Provincial 2011 Program (Collaborative  
435 Innovation Center of Climate Change).



## References

- Atkinson, J. D., Murray, B. J., Woodhouse, M. T., Whale, T. F., Baustian, K. J., Carslaw, K. S., Dobbie, S., O'Sullivan, D., and Malkin, T. L.: The importance of feldspar for ice nucleation by mineral dust in mixed-phase clouds, *Nature*, 498, 355-358, 10.1038/nature12278, 2013.
- 440 Awaka, J., Iguchi, T., Kumagai, H., Okamoto, K., and Ieee: Rain type classification algorithm for TRMM precipitation radar, 1997 International Geoscience and Remote Sensing Symposium (IGARSS 97) on Remote Sensing - A Scientific Vision for Sustainable Development, Singapore, Singapore, 1997, Aug 03-08, WOS:A1997BJ48Y00499, 1633-1635, 1997.
- Bellouin, N., Boucher, O., Haywood, J., and Reddy, M. S.: Global estimate of aerosol direct radiative  
445 forcing from satellite measurements, *Nature*, 438, 1138-1141, 10.1038/nature04348, 2005.
- Cao, Q. and Qi, Y.: The variability of vertical structure of precipitation in Huaihe River Basin of China: Implications from long-term spaceborne observations with TRMM precipitation radar, *Water Resour. Res.*, 50, 3690-3705, 10.1002/2013wr014555, 2014.
- Chen, T., Guo, J., Li, Z., Zhao, C., He, J.: A cloudsat perspective on the cloud climatology and its  
450 association with aerosol perturbations in the vertical over eastern china, *J. Atmos. Sci.*, 73(9), 10.1175/JAS-D-15-0309.1, 2016.
- DeMott, P. J., Prenni, A. J., Liu, X., Kreidenweis, S. M., Petters, M. D., Twohy, C. H., Richardson, M. S., Eidhammer, T., and Rogers, D. C.: Predicting global atmospheric ice nuclei distributions and their impacts on climate, *Proc. Natl. Acad. Sci. U. S. A.*, 107, 11217-11222, 10.1073/pnas.0910818107, 2010.
- 455 DeMott, P. J., Sassen, K., Poellot, M. R., Baumgardner, D., Rogers, D. C., Brooks, S. D., Prenni, A. J., and Kreidenweis, S. M.: African dust aerosols as atmospheric ice nuclei, *Geophys. Res. Lett.*, 30, 10.1029/2003gl017410, 2003.
- Dong, X., Li, R., Wang, Y., Fu, Y., and Zhao, C.: Potential Impacts of Sahara Dust Aerosol on Rainfall Vertical Structure Over the Atlantic Ocean as Identified From EOF Analysis, *J. Geophys. Res.-Atmos.*,  
460 123, 8850-8868, 10.1029/2018jd028500, 2018.
- Doswell, C. A. and Rasmussen, E. N.: THE EFFECT OF NEGLECTING THE VIRTUAL TEMPERATURE CORRECTION ON CAPE CALCULATIONS, *Weather Forecast.*, 9, 625-629, 10.1175/1520-0434(1994)009<0625:Teontv>2.0.Co;2, 1994.





- Fan, J., L. R. Leung, D. Rosenfeld, Q. Chen, Z. Li, J. Zhang, and H. Yan, 2013: Microphysical effects  
465 determine macrophysical response for aerosol impacts on deep convective clouds, *Proc. Natl. Acad. Sci.*  
U. S. A., 110, E4581–E4590, doi:10.1073/pnas.1316830110.
- Fan, J., Rosenfeld, D., Zhang, Y., Giangrande, S. E., Li, Z., Machado, L. A. T., Martin, S. T., Yang, Y.,  
Wang, J., Artaxo, P., Barbosa, H. M. J., Braga, R. C., Comstock, J. M., Feng, Z., Gao, W., Gomes, H. B.,  
Mei, F., Poehlker, C., Poehlker, M. L., Poeschl, U., and de Souza, R. A. F.: Substantial convection and  
470 precipitation enhancements by ultrafine aerosol particles, *Science*, 359, 411–+, 10.1126/science.aan8461,  
2018.
- Fan, J., Yuan, T., Comstock, J. M., Ghan, S., Khain, A., Leung, L. R., Li, Z., Martins, V. J., and  
Ovchinnikov, M.: Dominant role by vertical wind shear in regulating aerosol effects on deep convective  
clouds, *J. Geophys. Res.-Atmos*, 114, 10.1029/2009jd012352, 2009.
- 475 Fedorovich, E. and Conzemius, R.: Effects of wind shear on the atmospheric convective boundary layer  
structure and evolution, *Acta Geophys.*, 56, 114–141, 10.2478/s11600-007-0040-4, 2008.
- Gibbons, M., Min, Q., and Fan, J.: Investigating the impacts of Saharan dust on tropical deep convection  
using spectral bin microphysics, *Atmos. Chem. Phys.*, 18, 12161–12184, 10.5194/acp-18-12161-2018,  
2018.
- 480 Guo, J., Liu, H., Li, Z., Rosenfeld, D., Jiang, M., Xu, W., Jiang, J. H., He, J., Chen, D., Min, M.: Aerosol-  
induced changes in the vertical structure of precipitation: A perspective of TRMM precipitation radar,  
*Atmos. Chem. Phys.*, 18, 13329–13343, 10.5194/acp-2018-366, 2018.
- Houze, R. A.: Stratiform precipitation in regions of convection: A meteorological paradox?, *Bull. Amer.*  
*Meteorol. Soc.*, 78, 2179–2196, 10.1175/1520-0477(1997)078<2179:Spirc>2.0.Co;2, 1997.
- 485 Huang, J., Wang, T., Wang, W., Li, Z., and Yan, H.: Climate effects of dust aerosols over East Asian arid  
and semiarid regions, *J. Geophys. Res.-Atmos*, 119, 11398–11416, 10.1002/2014jd021796, 2014.
- Iguchi, T., Meneghini, R., Awaka, J., Kozu, T., and Okamoto, K.: Rain profiling algorithm for TRMM  
precipitation radar data, in: *Remote Sensing and Applications: Earth, Atmosphere and Oceans*, edited by:  
Igarashi, T., Nakamura, K., Shimoda, H., Tanaka, T., Burrows, J. P., Nakajima, T., Talagrand, O., and  
490 Naeije, M. C., *Advances in Space Research-Series*, 5, 973–976, 10.1016/s0273-1177(99)00933-3, 2000.



- Jones, T. A. and Christopher, S. A.: MODIS derived fine mode fraction characteristics of marine, dust, and anthropogenic aerosols over the ocean, constrained by GOCART, MOPITT, and TOMS, *J. Geophys. Res.-Atmos*, 112, 10.1029/2007jd008974, 2007.
- Khain, A. P.: Notes on state-of-the-art investigations of aerosol effects on precipitation: a critical review, *Environ. Res. Lett.*, 4, 10.1088/1748-9326/4/1/015004, 2009.
- Li, R. and Min, Q. L.: Impacts of mineral dust on the vertical structure of precipitation, *J. Geophys. Res.-Atmos*, 115, 10.1029/2009jd011925, 2010.
- Li, R., Dong, X., Guo, J., Fu, Y., Zhao, C., Wang, Y., and Min, Q.: The implications of dust ice nuclei effect on cloud top temperature in a complex mesoscale convective system, *Sci Rep*, 7, 10.1038/s41598-017-12681-0, 2017a.
- Li, R., Min, Q. L., and Harrison, L. C.: A Case Study: The Indirect Aerosol Effects of Mineral Dust on Warm Clouds, *J. Atmos. Sci.*, 67, 805-816, 10.1175/2009jas3235.1, 2010.
- Li, R., Min, Q., and Fu, Y.: 1997/98 El Nino-Induced Changes in Rainfall Vertical Structure in the East Pacific, *J. Clim.*, 24, 6373-6391, 10.1175/jcli-d-11-00002.1, 2011a.
- Li, R., Shao, W., Guo, J., Fu, Y., Wang, Y., Liu, G., Zhou, R., and Li, W.: A Simplified Algorithm to Estimate Latent Heating Rate Using Vertical Rainfall Profiles Over the Tibetan Plateau, *J. Geophys. Res.-Atmos*, 124, 942-963, 10.1029/2018jd029297, 2019a.
- Li, Z., Guo, J., Ding, A., Liao, H., Liu, J., Sun, Y., Wang, T., Xue, H., Zhang, H., and Zhu, B.: Aerosol and boundary-layer interactions and impact on air quality, *Natl. Sci. Rev.*, 4, 810-833, 10.1093/nsr/nwx117, 2017b.
- Li, Z., Niu, F., Fan, J., Liu, Y., Rosenfeld, D., and Ding, Y.: Long-term impacts of aerosols on the vertical development of clouds and precipitation, *Nat. Geosci.*, 4, 888-894, 10.1038/ngeo1313, 2011b.
- Li, Z., Wang, Y., Guo, J., Zhao, C., Cribb, M., Dong, X., Fan, J., Gong, D., Huang, J., Jiang, M., Jiang, Y., Lee, S. S., Li, H., Li, J., Liu, J., Qian, Y., Rosenfeld, D., Shan, S., Sun, Y., Wang, H., Xin, J., Yan, X., Yang, X., Yang, X.-q., Zhang, F., and Zheng, Y.: East Asian Study of Tropospheric Aerosols and their Impact on Regional Clouds, Precipitation, and Climate (EAST-AIR(CPC)), *J. Geophys. Res.-Atmos*, 124, 13026-13054, 10.1029/2019jd030758, 2019b.
- Liu, G. S. and Fu, Y. F.: The characteristics of tropical precipitation profiles as inferred from satellite radar measurements, *J. Meteorol. Soc. Jpn.*, 79, 131-143, 10.2151/jmsj.79.131, 2001.



- 520 Min, Q. L., Li, R., Lin, B., Joseph, E., Wang, S., Hu, Y., Morris, V., and Chang, F.: Evidence of mineral dust altering cloud microphysics and precipitation, *Atmos. Chem. Phys.*, 9, 3223-3231, 10.5194/acp-9-3223-2009, 2009.
- Nasuno, T. and Satoh, M.: Properties of Precipitation and In-Cloud Vertical Motion in a Global Nonhydrostatic Aquaplanet Experiment, *J. Meteorol. Soc. Jpn.*, 89, 413-439, 10.2151/jmsj.2011-502, 525 2011.
- Oshima, N., Kondo, Y., Moteki, N., Takegawa, N., Koike, M., Kita, K., Matsui, H., Kajino, M., Nakamura, H., Jung, J. S., and Kim, Y. J.: Wet removal of black carbon in Asian outflow: Aerosol Radiative Forcing in East Asia (A-FORCE) aircraft campaign, *J. Geophys. Res.-Atmos.*, 117, 10.1029/2011jd016552, 2012.
- Park, S. and Allen, R. J.: Understanding influences of convective transport and removal processes on 530 aerosol vertical distribution, *Geophys. Res. Lett.*, 42, 10438-10444, 10.1002/2015gl066175, 2015.
- Prospero, J. M. and Mayol-Bracero, O. L.: UNDERSTANDING THE TRANSPORT AND IMPACT OF AFRICAN DUST ON THE CARIBBEAN BASIN, *Bull. Amer. Meteorol. Soc.*, 94, 1329-1337, 10.1175/bams-d-12-00142.1, 2013.
- Rosenfeld, D., Andreae, M. O., Asmi, A., Chin, M., de Leeuw, G., Donovan, D. P., Kahn, R., Kinne, S., 535 Kivekas, N., Kulmala, M., Lau, W., Schmidt, K. S., Suni, T., Wagner, T., Wild, M., and Quaas, J.: Global observations of aerosol-cloud-precipitation-climate interactions, *Rev. Geophys.*, 52, 750-808, 10.1002/2013rg000441, 2014.
- Rosenfeld, D., Lohmann, U., Raga, G. B., O'Dowd, C. D., Kulmala, M., Fuzzi, S., Reissell, A., and Andreae, M. O.: Flood or drought: How do aerosols affect precipitation?, *Science*, 321, 1309-1313, 540 10.1126/science.1160606, 2008.
- Shige, S., Takayabu, Y. N., Tao, W. K., and Johnson, D. E.: Spectral retrieval of latent heating profiles from TRMM PR data. Part I: Development of a model-based algorithm, *J. Appl. Meteorol.*, 43, 1095-1113, 10.1175/1520-0450(2004)043<1095:Srollhp>2.0.Co;2, 2004.
- Shige, S., Takayabu, Y. N., Tao, W.-K., and Shie, C.-L.: Spectral retrieval of latent heating profiles from 545 TRMM PR data. Part II: Algorithm improvement and heating estimates over Tropical Ocean regions, *J. Appl. Meteorol. Climatol.*, 46, 1098-1124, 10.1175/jam2510.1, 2007.



- Tao, W. K., Lang, S., Simpson, J., and Adler, R.: RETRIEVAL ALGORITHMS FOR ESTIMATING THE VERTICAL PROFILES OF LATENT-HEAT RELEASE - THEIR APPLICATIONS FOR TRMM, *J. Meteorol. Soc. Jpn.*, 71, 685-700, 10.2151/jmsj1965.71.6\_685, 1993.
- 550 Tao, W.-K., Lang, S., Zeng, X., Shige, S., and Takayabu, Y.: Relating Convective and Stratiform Rain to Latent Heating, *J. Clim.*, 23, 1874-1893, 10.1175/2009jcli3278.1, 2010.
- Teller, A. and Levin, Z.: The effects of aerosols on precipitation and dimensions of subtropical clouds: a sensitivity study using a numerical cloud model, *Atmos. Chem. Phys.*, 6, 67-80, 10.5194/acp-6-67-2006, 2006.
- 555 Wall, C., Zipser, E., and Liu, C.: An Investigation of the Aerosol Indirect Effect on Convective Intensity Using Satellite Observations, *J. Atmos. Sci.*, 71, 430-447, 2015.
- Yin, Y. and Chen, L.: The effects of heating by transported dust layers on cloud and precipitation: a numerical study, *Atmos. Chem. Phys.*, 7, 3497-3505, 10.5194/acp-7-3497-2007, 2007.
- Yin, Y., Chen, Q., Jin, L., Chen, B., Zhu, S., and Zhang, X.: The effects of deep convection on the concentration and size distribution of aerosol particles within the upper troposphere: A case study, *J. Geophys. Res.-Atmos.*, 117, 10.1029/2012jd017827, 2012.
- 560 Zhang, D., Wang, Z., Heymsfield, A., Fan, J., Liu, D., and Zhao, M.: Quantifying the impact of dust on heterogeneous ice generation in midlevel supercooled stratiform clouds, *Geophys. Res. Lett.*, 39, 10.1029/2012gl052831, 2012.
- 565

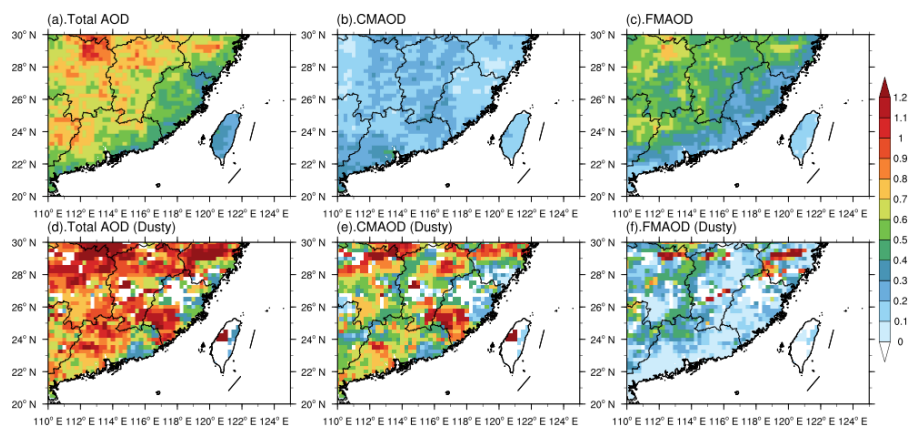
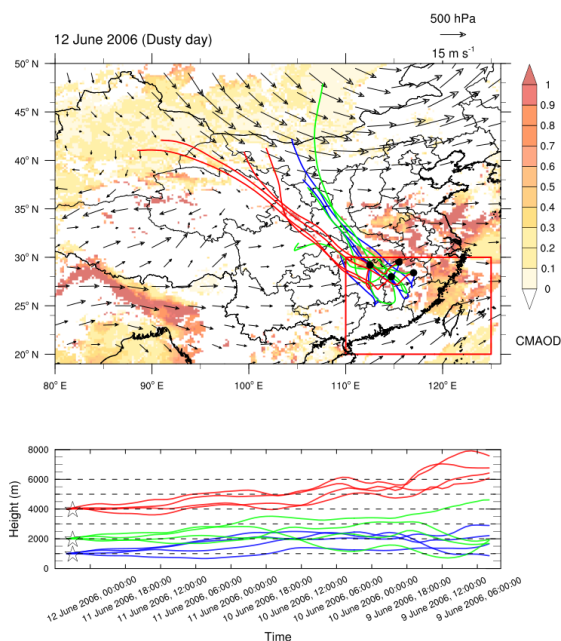


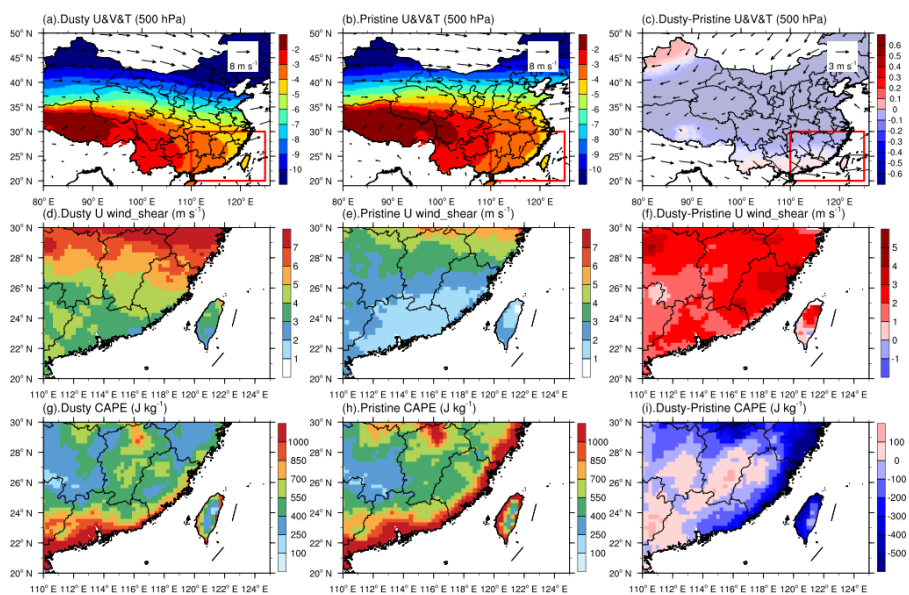
**Figure 1:** Total aerosol optical depth (a, d), coarse mode aerosol optical depth (CMAOD, b, e), and fine mode aerosol optical depth (FMAOD, c, f) under all days (the first row), and dusty days (the second row) in June, July and August (JJA) during 2000 to 2013 retrieved from Terra MODIS.

570

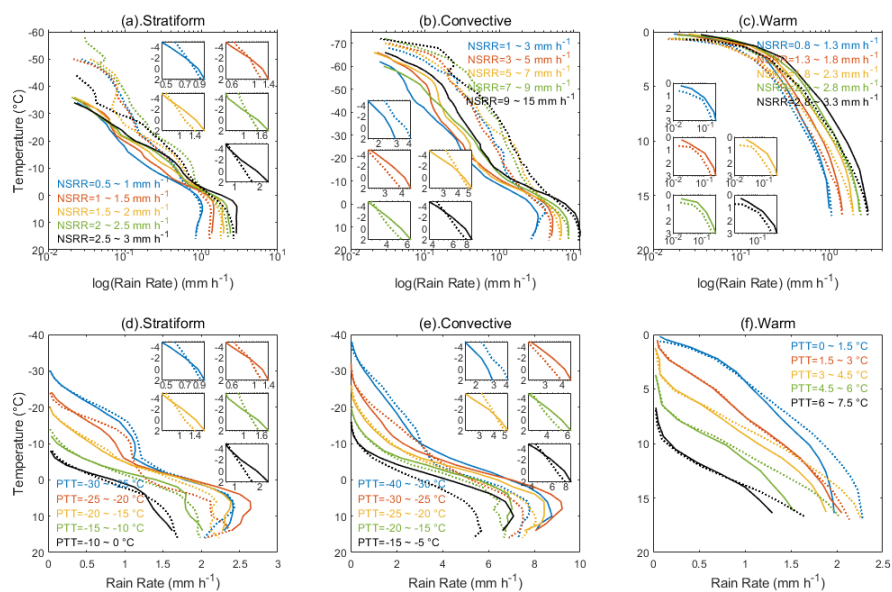


575

**Figure 2:** Horizontal distribution of coarse mode aerosol optical depth derived from Terra MODIS, wind fields at 500 hPa, and 72-hour back trajectories from the HYSPLIT model on 12 June 2006. Where the red box indicates the study area, the geolocation of four starting points are at 29.5° N, 115.5° E; 28° N, 114.7° E; 28.4° N, 117° E; and 29.2° N, 112.5° E, with altitudes of 1000 m (blue line), 2000 m (green line), and 4000 m (red line), extrapolated from 12 June 2006 at 04:00 UTC.



580 **Figure 3:** The mean fields of wind and temperature at 500 hPa (upper row), U wind shear (middle row), CAPE (bottom row) for dusty (left column) and pristine (middle column), and the associated differences (dusty minus pristine, right column).



585 **Figure 4:** Differences in vertical profiles of stratiform (a,d), convective (b,e) and warm (c,f) precipitation for pristine (dashed line) and dusty (solid line) conditions for given NSRR (the first row) and PTT (the second row). Different color stands for different NSRR and PTT. Each subpanel focuses on the rain rate in the mixed layer (temperatures between -5 °C to 2 °C).





590

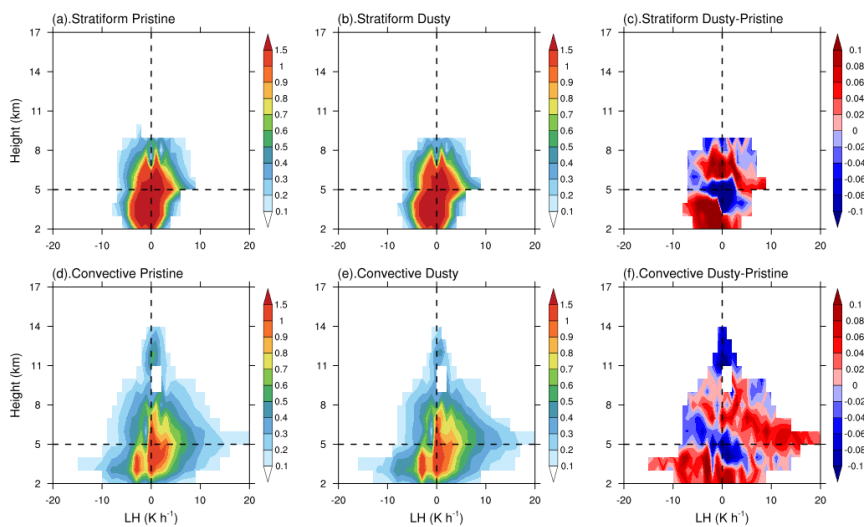


**Figure 5: Contoured frequency by altitude diagrams (CFADs) of LH (retrieval from VPH) in pristine (the first column) conditions, dusty (the second column) conditions and the differences between them (the third column) for stratiform (the first row) and convective (the second row) rains.**

595

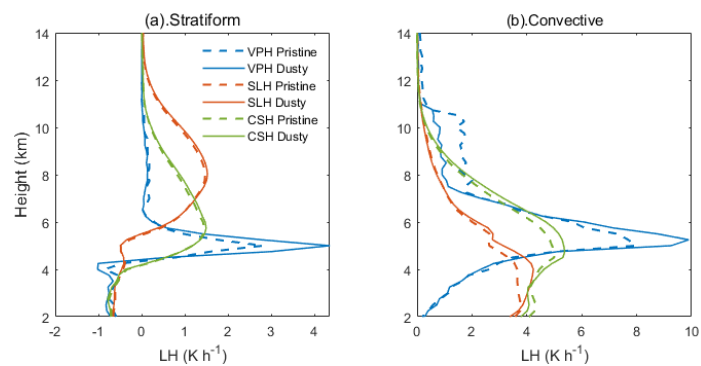
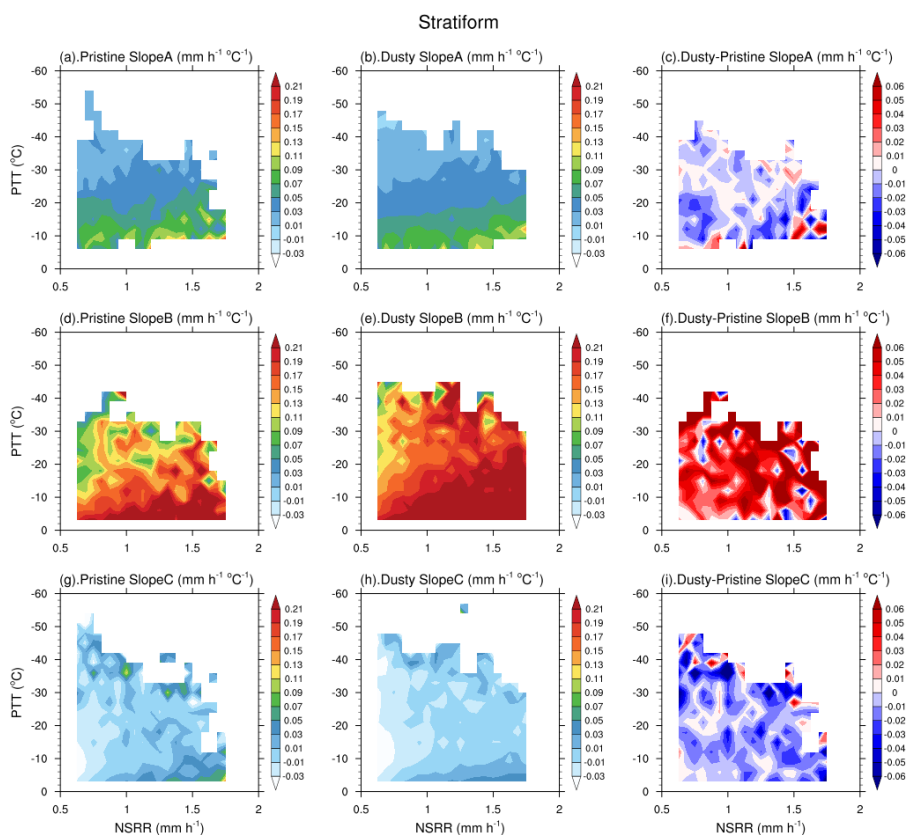


**Figure 6:** The mean latent heating (LH) profiles retrieved from VPH (blue), SLH (red) and CSH (green) for (a) stratiform precipitation and (b) convective precipitation in pristine (dashed) and dusty (solid) conditions.



600

**Figure 7: The mean SlopeA (the first row), SlopeB (the second row), and SlopeC (the third row) for stratiform precipitation as functions of near surface rain rate (NSRR) and precipitation top temperature (PTT) in pristine (the left column) conditions, dusty (the middle column) conditions and the differences between them (dusty minus pristine, the right column).**

605

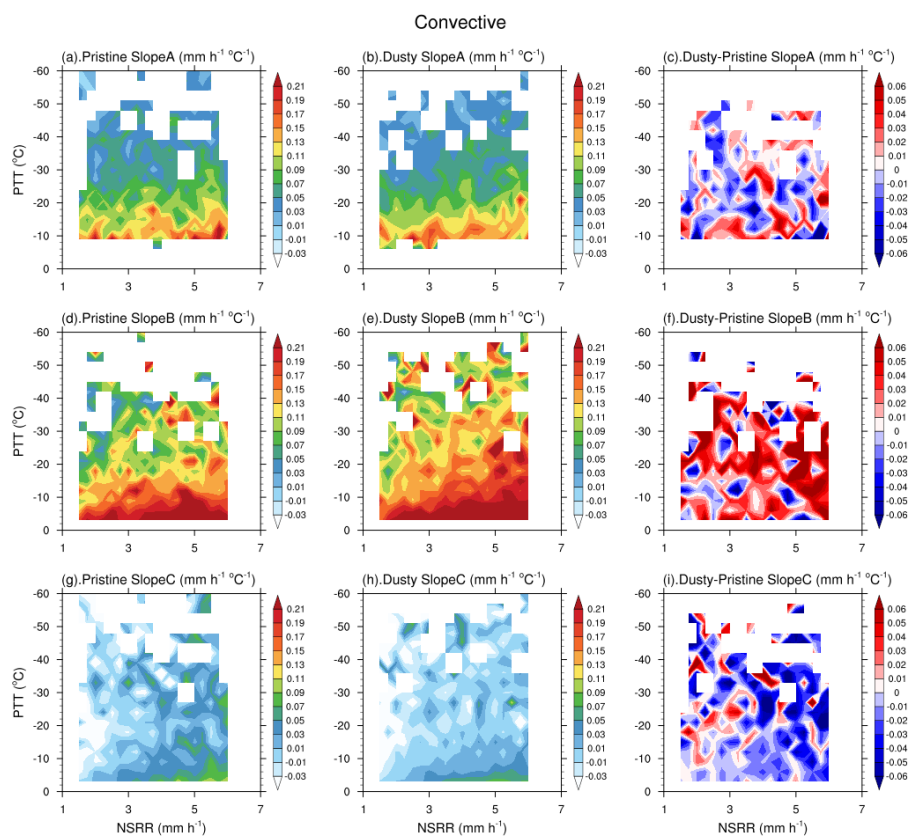
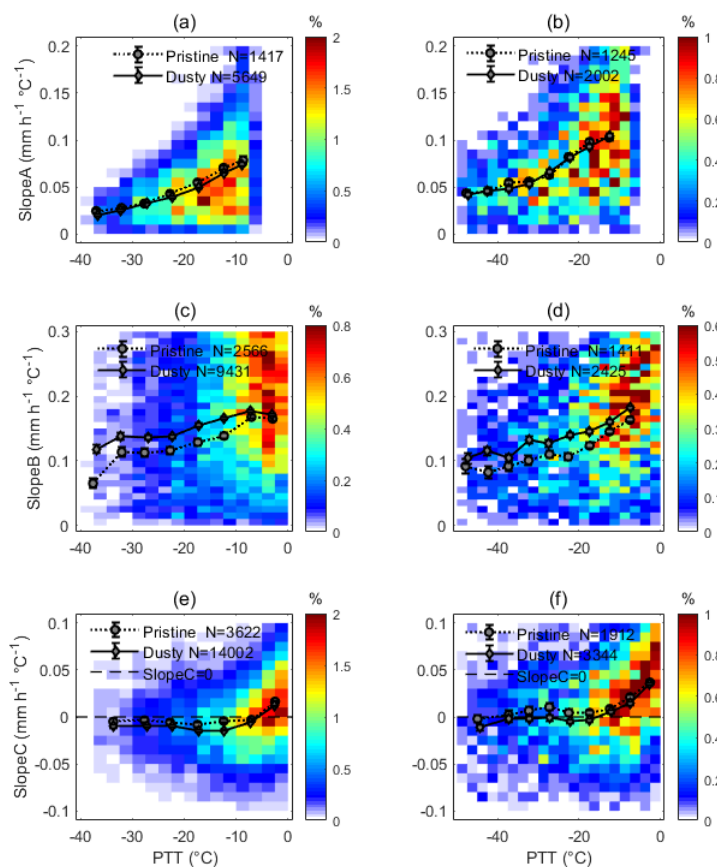
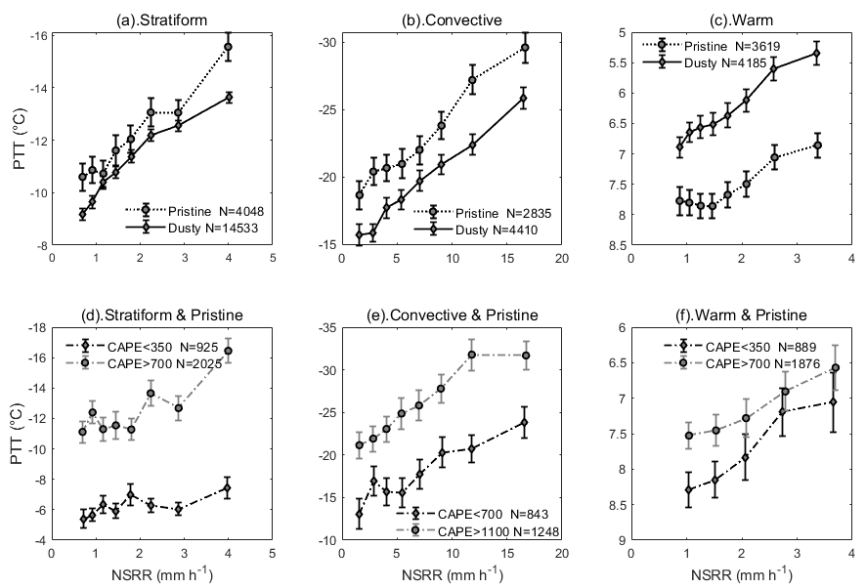


**Figure 8:** As same as Figure 7, but for deep convective precipitation.



610 **Figure 9:** The mean Slope A (a, b), Slope B (c, d) and Slope C (e, f) as functions of precipitation top temperature (PTT) for stratiform (the first column) and convective (the second column) rains under pristine (dotted line) and dusty (solid line) conditions. Overlapped are the contoured occur frequency (%) of samples under dusty conditions.



615

**Figure 10:** The precipitation top temperature (PTT) against near surface rain rate (NSRR) for stratiform (a, d), convective (b, e) and warm (c, f) precipitation under pristine (dotted curves) and dusty (solid curves) conditions (the first row) and in different CAPE (black line: weak CAPE, gray line: strong CAPE) conditions under pristine conditions (the second row).

620

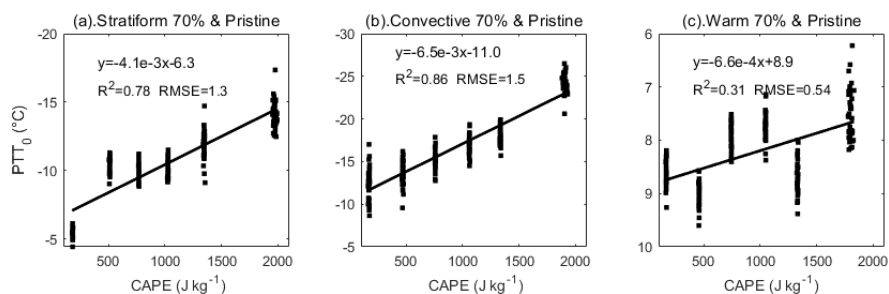


**Figure 11:** The variation of  $PTT_0$  with CAPE under pristine condition for (a) deep stratiform precipitation; (b) deep convective precipitation and (c) warm rains.